Hindawi
Journal of Nanomaterials
Volume 2019, Article ID 7586790, 10 pages
https://doi.org/10.1155/2019/7586790

Research Article

Enhancement of the Electrochemical Performance of $LiNi_{1/3}Co_{1/3}Mn_{1/3}O_2$ Cathode Material by Double-Layer Coating with Graphene Oxide and SnO_2 for Lithium-Ion Batteries

Yuxin Ma,[1,2] Ping Cui,[1] Dan Zhan,[1] Bing Gan,[1] Youliang Ma,[2] and Ying Liang[1,2]

[1]*School of Chemical Engineering, Hubei University of Arts and Science, Xiangyang 441053, China*
[2]*School of Automobile and Traffic Engineering, Wuhan University of Science and Technology, Wuhan 430081, China*

Correspondence should be addressed to Ying Liang; xfliangy@163.com

Received 1 December 2018; Revised 7 February 2019; Accepted 17 February 2019; Published 22 April 2019

Academic Editor: Ungyu Paik

The graphene oxide-coated SnO_2-$Li_{1/3}Co_{1/3}Mn_{1/3}O_2$ (GO-SnO_2-NCM) cathode material was successfully synthesized via a facile wet chemical method. The pristine NCM and GO-SnO_2-NCM were characterized by X-ray diffraction, scanning electron microscopy, energy-dispersive spectroscopy, transmission electron microscopy, and X-ray photoelectron spectroscopy. The results showed that the double-coating layer did not destroy the NCM crystal structure, with multiple nano-SnO_2 particles and GO uniformly covering the NCM surface. Electrochemical tests indicated that GO-SnO_2-NCM exhibited excellent cycling performance, with 90.7% capacity retention at 1 C after 100 cycles, which was higher than 74.3% for the pristine NCM at the same cycle. The rate capability showed that the double-coating layer enhanced surface electronic–ionic transport. Electrochemical impedance spectroscopy results confirmed that the GO-SnO_2-coating layer effectively suppressed the increased electrode polarization and charge transfer resistance during cycling.

1. Introduction

Current methods for addressing the global energy crisis and serious climate change issues require the development of sustainable and high-performance storage equipment, such as lithium-ion batteries [1], sodium–sulfur batteries [2], supercapacitors [3], solar cells [4], and fuel cells [5]. Advanced lithium-ion batteries have been widely used as power sources in battery electric vehicles, hybrid electric vehicles (HEVs), and parallel HEVs because of their advantages of high energy density, high power capability, low cost, long life cycle, and environmental friendliness [6–8]. Lithium-ion batteries are mainly composed of cathodes, anodes, and electrolytes. Cathode materials play a significant role in determining battery performance. As the cathode material for the first generation of lithium-ion batteries, $LiCoO_2$ has the advantages of easy synthesis, excellent cycling stability, and high rate capability [9]. Only half of the theoretical capacity can be utilized because of structure degradation when $LiCoO_2$cathode is charged at 4.2 V. Additionally, its high cost, poor thermal stability, and toxicity limit the large-scale application of $LiCoO_2$ commercially. $LiNiO_2$ [10] is considered as a second-generation commercial lithium-ion battery owing to high power, energy density, low cost, and high discharge capacity; however, it is difficult to synthesize $LiNiO_2$ because of the chemical instability of Ni^{3+} ions. $LiMn_2O_4$ [11] provides high thermal stability and high voltage and has a low cost; it exhibits poor performance at high temperatures.

Recently, layered $LiNi_{1-x-y}Co_xMn_yO_2$ material has earned much interest because it combines the merits of $LiCoO_2$, $LiNiO_2$, and $LiMn_2O_4$ and overcomes certain shortcomings associated with each material. The amount of Ni represents the specific capacity and an increase in Ni content results in the deterioration of electrochemical performance owing to the cation mixing. Typically, $LiNi_{1/3}Co_{1/3}Mn_{1/3}O_2$ is considered a promising cathode material that exhibits high discharge capacity, has low cost, and represents a moderate voltage platform. The electrochemical inactivity of tetravalent manganese plays a stabilizing role in preventing capacity fading induced by Mn dissolution. The cobalt reduces cation

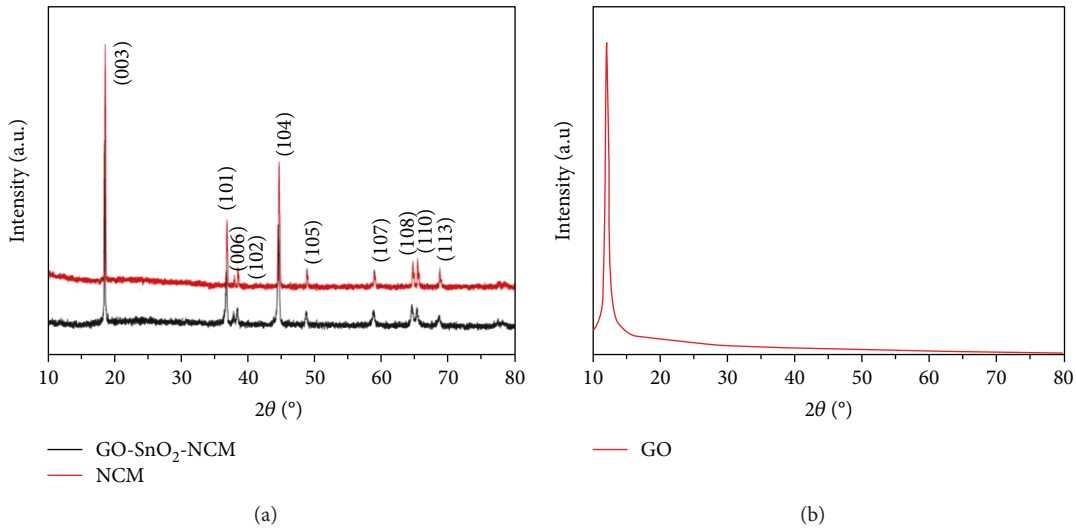

Figure 1: XRD patterns of pristine NCM and GO-SnO_2-NCM (a) and GO (b).

mixing and prohibits charge forming in the structure of the cathode material during cycling [12]. In particular, there are several substantial issues such as inevitable capacity degradation, poor rate capability, and bad cyclability that originate from the severed side reaction between the electrode and electrolyte.

Many strategies have been explored to reduce the side reaction and improve electrochemical performance, particularly the rate capability and cycle performance of cathode materials. Surface modification is one of the most facile and practical approaches, which is capable of effectively suppressing solid electrolyte interphase layer growth and maintaining the surface integrity of cathode materials. Presently, the most common coating materials include metal oxides such as Nb_2O_5 [13], Al_2O_3 [14], ZrO_2 [15], and TiO_2 [16] and metal phosphates such as Li_3PO_4 [17] and $AlPO_4$ [18], which have been successfully applied on the surface of NCM to improve the electrochemical performance. Most of the aforementioned coating layers are inactive substances that only function as protective shells, which will result in polarization increasing and capacity decreasing. Another approach to enhance electrochemical performance of the NCM cathode material focused on reducing both NCM and coating layers on nanoparticles. SnO_2 can react with Li reversibly by a conversion reaction and has been used to coat on the NCM surface [19].

GO-coated cathode materials were used to improve electrochemical performance based on their superior electronic conductivity and large surface area [20, 21]. In this study, a double-coating layer structure including an inner SnO_2 nanosize and an outer GO layer was introduced to coat the NCM cathode material. The inner SnO_2 not only promoted lithium-ion diffusivities but also suppressed the side reaction between electrode and electrolyte; the outer GO layer increased the electronic conductivity on the surface of the NCM. The pristine NCM was modified with SnO_2 and GO, with electrochemical results revealing that the GO-SnO_2 double-coating layer on the surface of the NCM cathode material exhibited high rate capability and long-term cyclability when compared with pristine NCM powders. A detailed comparison of the performance of NCM and the GO-SnO_2-NCM composite was performed.

Table 1: Lattice parameters and relative intensities of the pristine NCM and GO-SnO_2-NCM.

Sample	a (Å)	c (Å)	c/a	$I_{(003)}/I_{(104)}$
NCM	2.857	14.205	4.972	1.28
GO-SnO_2-NCM	2.861	14.239	4.977	1.35

2. Experimental

2.1. NCM Synthesis. NCM was synthesized via a sol–gel citric acid-assisted method. Lithium acetate, nickel acetate, cobalt acetate, and manganese acetate were chosen as the starting materials, with a stoichiometric ratio of Li(Ni+Co+Mn)(=1.05 : 1) dissolved in ethyl alcohol. Excess 5% Li^+ was added to supplement the loss, which occurred at high temperatures. Citric acid solution was added dropwise into the above solution with vigorous stirring. The molar ratio of metal ions to citric acid was 1 : 1. The mixture was evaporated at 80°C with continuous stirring until a gel formed; the gel was frozen at -80°C in a cryogenic refrigerator for 12 h, followed by a freeze-drying for 24 h to acquire the precursor. The precursor was heated at 450°C in air for 5 h, with subsequent calcinations at 900°C for 12 h to obtain the pristine NCM.

2.2. Synthesis of GO-SnO_2-NCM. GO was produced via the modified Hummers method [22, 23]. GO-coated SnO_2-NCM material was prepared via a facile wet chemical method. First, $SnCl_4 \cdot 5H_2O$ was added into 100 mL ethanol using ultrasonic treatment for 1 h; second, 1 g NCM cathode material was dispersed into the above solution and stirring for 2 h; third, an adequate amount of $NH_3 \cdot H_2O$ was induced

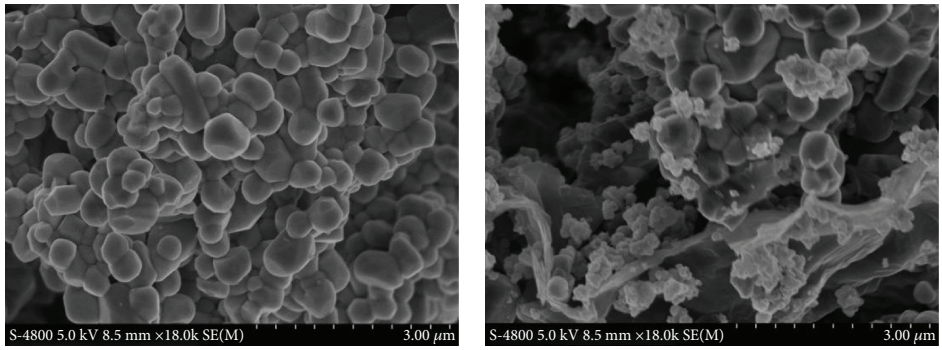

(a) (b)

Figure 2: SEM images of pristine NCM (a) and GO-SnO_2-NCM cathodes (b).

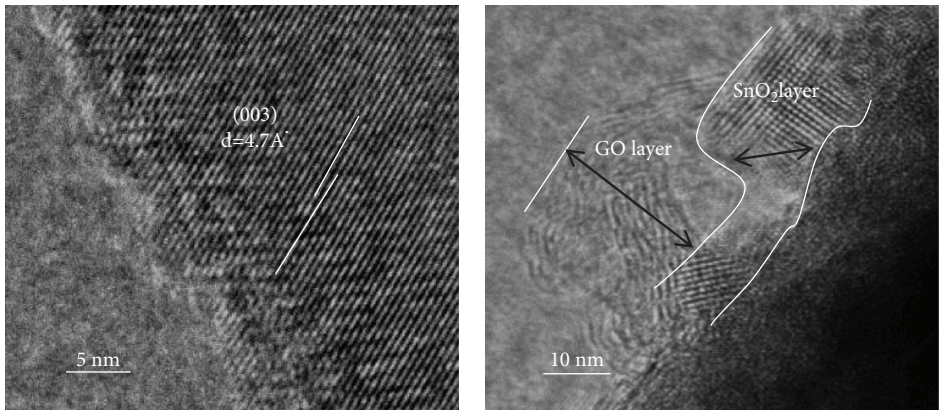

(a) (b)

Figure 3: HRTEM micrographs of NCM (a) and GO-SnO_2-NCM powders (b).

to form a precipitate. The resulting mixture was filtered with deionized water/ethanol (1 : 1 *v*/*v*) three times and dried for 12 h at 80°C. The dried powder was heat-treated in a furnace at 500°C for 6 h in air atmosphere. GO (0.03 g) was immersed into 50 mL of anhydrous ethanol and sonicated for 2 h to ensure complete dispersal. SnO_2-NCM was added in the above solution with constant stirring, and the mixture was heated at 80°C until the ethanol was completely evaporated. The powder was dried at 80°C for 4 h in a vacuum to obtain GO-SnO_2-NCM materials.

2.3. Material Characterization. The crystal structure was analyzed via X-ray diffraction (D8 advance, Bruker) with Cu-Kα radiation (40 kV, 40 mA) in the 2θ range of 10°–80° at a scan rate of 10°/min. The particle size, surface morphologies, and elemental composition of the samples were analyzed via scanning electron microscopy (SEM, S-4800, Hitachi) equipped with an energy-dispersive spectroscope (EDS). Transmission electron microscopy (TEM, Talos F200S, FEI) was used to estimate the thickness coated on the surface of the cathode powders. X-ray photoelectron spectroscopy (XPS, ESCALAB 250Xi, Thermo Fisher Scientific) was utilized to evaluate the ion valence states in the metal oxide.

2.4. Electrochemical Measurements. The electrochemical properties of pristine NCM and GO-SnO_2-modified NCM were measured using a CR2032 coin cell. The electrodes were prepared by mixing the active material with acetylene black and polyvinylidene fluoride at a mass ratio of 80 : 10 : 10 in N-methyl-2-pyrrolidone to obtain a slurry, which was coated onto a cleaned and polished aluminum foil and then dried at 80°C for 10 h in a vacuum oven. The cells were assembled in an argon-filled glove box, in which water and oxygen levels were maintained below 1 ppm. $LiPF_6$ (1 M) was dissolved in EC:DMC (1 : 1 *v*/*v*%) as the electrolyte. The cells consist of a prepared cathode, with lithium metal as an anode and a polypropylene microporous film (Celgard 2400) as the separator. A galvanostatic change–discharge test was performed at C (1 C = 280 mA g^{-1}) rates of 0.2, 0.5, 1, 2, and 5 in the voltage range of 2.5–4.3 V at 25°C. Electrochemical impedance spectroscopy (EIS) tests were performed on an Autolab PGSTAT 302N at a frequency range of 0.01 Hz to 100 kHz with a potential perturbation of 5 mV.

3. Results and Discussion

Figure 1 shows the XRD patterns of the pristine NCM and GO-SnO_2-NCM. It can be seen that a sharp peak at 11°

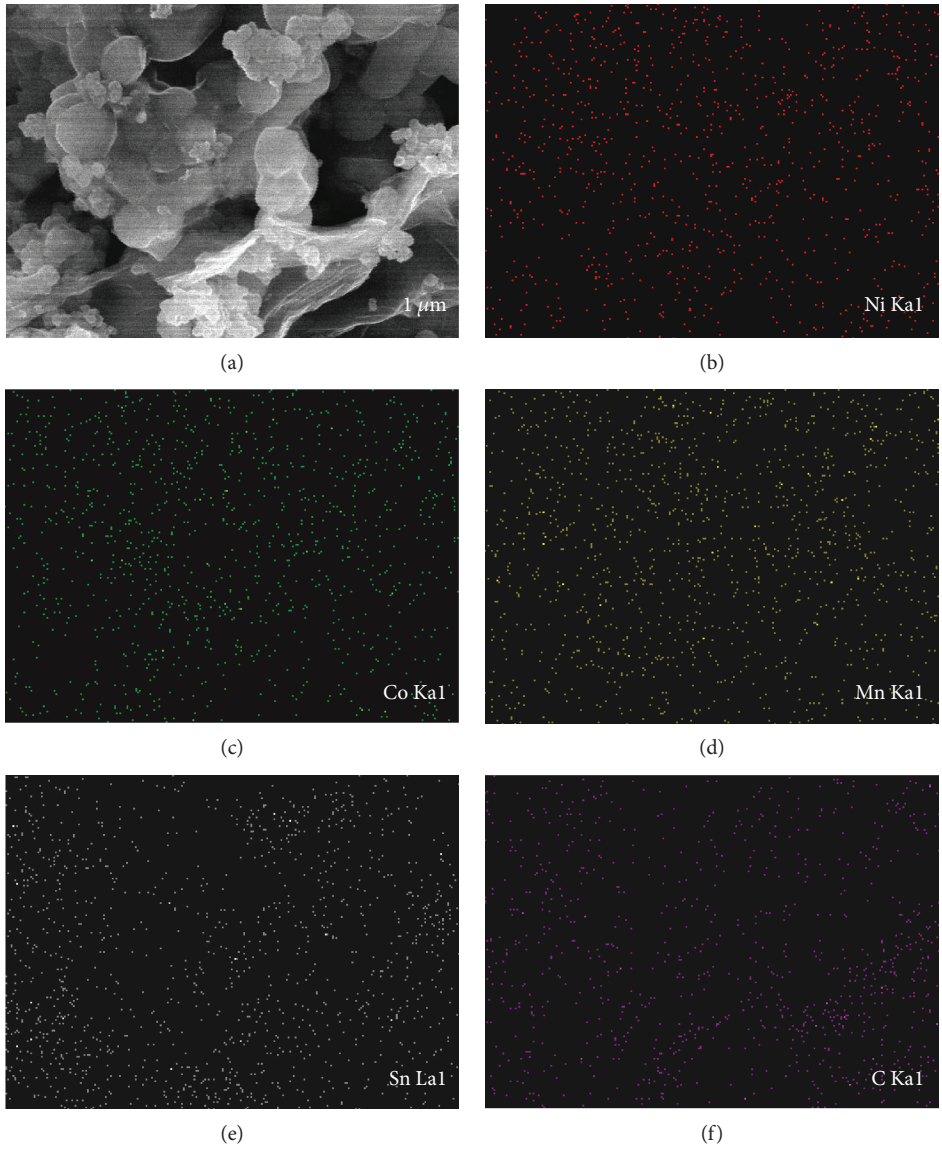

Figure 4: EDS maps of the GO-SnO_2-NCM.

corresponds to complete oxidation of graphite (GO) [24]. The synthesized materials exhibited similar XRD patterns with no impurity phase detected, and these patterns could be indexed to the hexagonal -$NaFeO_2$ structure with a space group of $R\bar{3}m$. The clear splitting of peaks (006)/(102) and (108)/(110) near 38° and 65°, respectively, exhibits a perfect layered structure [25]. The diffraction peaks of the material show no significant difference before or after coating, because the coated amount was below the election limit of the instrument or the nanoscale size feature of the low-content GO-SnO_2 content [26]. The ionic radius of Ni^{2+} ($r = 0.69$ Å) is similar to Li^+ ($r = 0.76$ Å), and portions of Ni^{2+} might occupy the 3a site, which indicates cation mixing. The intensity of $I_{(003)}/I_{(104)}$ is a sensitivity parameter focused on the degree of cation mixing of the materials. When the ratio of $I_{(003)}/I_{(104)} > 1.2$, the degree of cation mixing is small [27]. The intensity ratio of $I_{(003)}/I_{(104)}$ for NCM and the GO-SnO_2-NCM samples was calculated as 1.28 and 1.35, respectively, which displays that the sample possessed a well-layered structure with a low degree of cation mixing. The lattice parameter constants for these materials are shown in Table 1. Additionally, a value of c/a above 4.9 implies that the material exhibits a well-defined layered structure [28]. It was clear that the as-synthesized GO-SnO_2-NCM increased the ordering degree of the layered structure and decreased the cation mixing in all samples.

The morphologies of NCM and GO-SnO_2-NCM were observed via SEM. Figure 2(a) shows that pristine NCM displayed homogeneous primary particles of the order of a few hundred nanometers, with few agglomerations. From the GO-SnO_2-NCM image (Figure 2(b)), the nanosize SnO_2-coated NCM particles were covered with a transparent GO sheet. The uniform GO-SnO_2-NCM structures can be ascribed to the simple chemical mixing method. Moreover, ultrasonication and continuous stirring were effective in distributing SnO_2-NCM throughout the GO sheets.

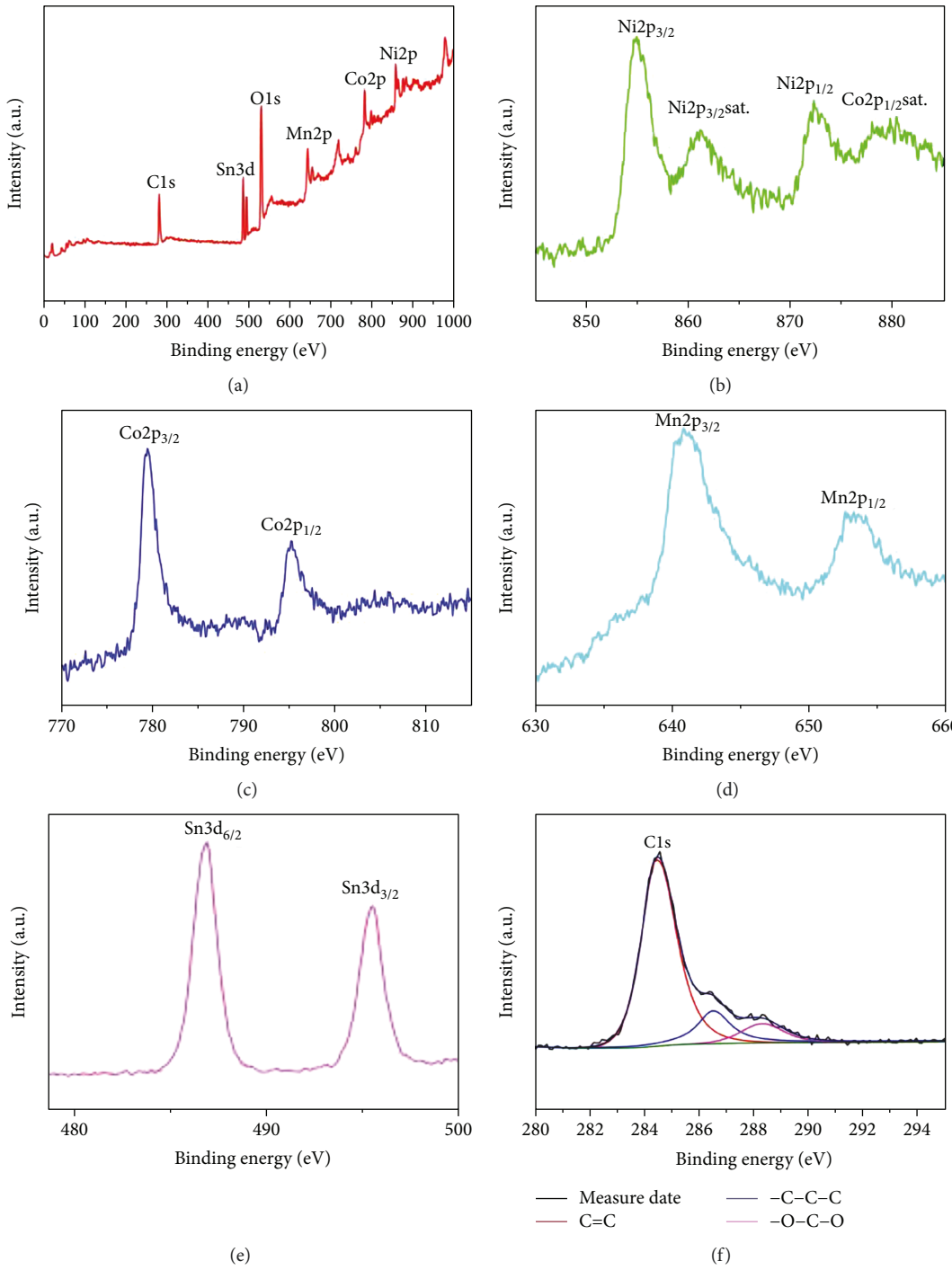

Figure 5: XPS spectra of the GO-SnO_2-NCM all elements (a), Ni2p(b), Co2p (c), Mn2p (d), Sn3p (e), and C1s (f).

To further study the microstructure of the material, high-resolution TEM (HRTEM) was used to characterize results (Figure 3). Figure 3(a) shows that pristine NCM presented fine crystallinity with an obvious lattice fringe extending to the particle boundary. HRTEM images display that the lattice fringe was about 0.47 nm, which corresponded to the (003) lattice plane of NCM. The outer coating layer, with a thickness of approximately 15 nm, belongs to the GO layer; the inner coating layer, with a thickness of approximately 5–10 nm, represents the SnO_2 layer, as shown in Figure 3(b). The SnO_2 particles with good electrical conductivity can effectively increase the conductivity of the samples. The GO sheets were not only covered with SnO_2 but also connected with NCM, which aids in improving material conductivity. Therefore, it could be identified that the double-coated layer not only increased the contact areas between electrode and electrolyte but also accelerated the electron transport speed of Li^+ ions.

EDS was used to confirm the elemental distribution of the GO-SnO_2-coated layer on the surface of NCM (Figure 4).

Results showed that the Sn element from SnO_2 and the C from GO were uniformly distributed on the NCM surface, which indicates that SnO_2 and GO were coated successfully on the NCM surface via coprecipitation and a simple chemical approach, respectively.

The modification of NCM with GO and SnO_2 can lead to the transition metals changing their oxidation states and issue in low discharge capacity and poor cycling performance. To confirm the valence state of the transition metal in the layered composite material, XPS analysis of GO-SnO_2-NCM was performed (Figure 5) and revealed that the electron-binding energies of $Ni2p_{1/2}$ and $Ni2p_{3/2}$ appeared at 872.6 and 855.6 eV, which implied that the Ni ion maintained its high oxidation state [29]. The satellite peak with a binding energy at 861.2 eV can be attributed to the multiple splitting of the nickel oxide energy levels [30]. The corresponding results indicated that the ionic radius of Ni^{2+} was close to that of Li^+; therefore, Ni^{2+} was easily located with regard to Li^+, which agreed with the XRD results. Additionally, peaks with binding energies of 780.1 and 642.5 eV were assigned to $Co2p_{3/2}$ and $Mn2p_{3/2}$, which accorded with previous reports [31]. These results suggested that the valence state of Co and Mn after coating remained trivalent and tetravalent, respectively. Two major peaks at 487.2 and 495.6 eV emerged in the GO-SnO_2-NCM sample, which corresponded to the $Sn3d_{5/2}$ and $Sn3d_{3/2}$ peaks and indicated the existence of an SnO_2-coating layer on the samples and the tetravalent status of Sn [32]. The C1s spectra of the materials were deconvoluted into three main peaks. These peaks having binding energies of 288.5, 286.6, and 285.6 eV were ascribed to a carboxyl group (C=O), an epoxide group (–C–O–C), and a hydroxyl group (C–OH), respectively [33]. These results suggested that the GO-SnO_2-coating layer on the surface of NCM did not change the valence state of the transition metal.

The initial charge–discharge curves of NCM and GO-SnO_2-NCM at 0.1 C over the potential range of 2.5–4.3 V are shown in Figure 6. All charge–discharge curves exhibited typical potential plateaus (3.6–3.8 V) associated with layered NCM, which was attributed to the Ni^{2+}/Ni^{3+} redox process [34]. For the NCM and GO-SnO_2-NCM composite, the charge and discharge capacities were 190.7/172.6 mAh g^{-1} and 210.3/197.2 mAh g^{-1}, respectively. The coulombic efficiency of coated NCM was 94%, which exceeded that of the pristine sample. This phenomenon indicates that the degree of cell polarization decreased. The GO-SnO_2-coating layer protected the surface of cathode particles from the liquid electrolyte and unwanted side reactions.

Figure 7(a) shows the cycle performance of the pristine NCM and GO-SnO_2-NCM materials at a constant current of 0.2 C and from 2.5 to 4.3 V at room temperature. The initial discharge capacity of the pristine NCM was 165.8 mAh g^{-1}, which sharply decreased to 140.3 mAh g^{-1} after 100 cycles, with capacity retention of 84.6%. However, GO-SnO_2-NCM not only increased the initial discharge capacity but also showed a high capacity retention of 93.5% after 100 cycles. These results indicated that the SnO_2-coating layer along with a GO-coating layer on the surface of NCM enhanced cycling stability and capacity retention.

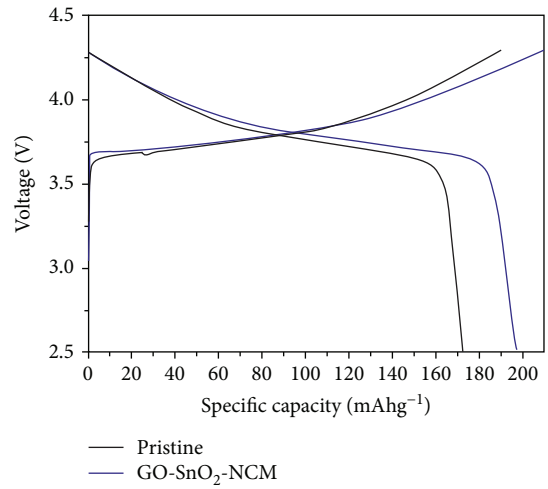

Figure 6: Initial charge–discharge curves for pristine NCM and GO-SnO_2-NCM samples.

To verify the cycling performance and capacity retention at high rates, the pristine NCM and GO-SnO_2-NCM cells were tested with a constant current density of 1 C between 2.5 and 4.3 V. After 100 charge–discharge cycles, the specific discharge capacity of the pristine NCM was 115.1 mAh g^{-1}, with a retention of 74.3% of its initial capacity (Figure 7(b)). However, the specific discharge capacity of GO-SnO_2-NCM was 158.1 mAh g^{-1}, which retained around 90.7% of the initial discharge capacity. The significant enhancement in the cycling performance and capacity retention of GO-SnO_2-NCM at 1 C can be ascribed to the following factors. First, the GO framework played a huge role in improving electrode conductivity during the process of charge transfer. Second, the nanosized SnO_2 prevented the cathode material from dissolution and suppressed interfacial impedance and electrode polarization; the results could be verified by subsequent EIS test. Third, the GO-SnO_2 double-coating layer suppressed the volume change and agglomeration during the cycling process.

The rate capabilities of NCM and GO-SnO_2-NCM samples were investigated. The charge–discharge processes were measured at a rate of 0.2 C, increased to 5 C step-wise, before finally returning to 0.2 C (Figure 8). Both the discharge capacity of NCM and that of GO-SnO_2-NCM decreased along with the increase in the current rate. The GO-SnO_2-NCM samples distinctly exhibited improvement of discharge capacities as compared with the pristine samples at high rates, with the former releasing 119.3 mAh g^{-1} under a high current rate of 5 C, while the pristine NCM remained at 90.8 mAh g^{-1}. Additionally, after cycling again at the low current rate of 0.2 C, the GO-SnO_2-NCM material maintained a higher capacity of 181.5 mAh g^{-1} than that of pristine NCM that had a capacity of 160.8 mAh g^{-1}. There are two main factors that affect the rate capacity of GO-SnO_2-NCM. The first factor is that the large number of NCM nanoparticles distributed within SnO_2 can shorten the electron transport path as well as strengthen the volume structure during the lithium-ion insertion/extraction process. The second factor is that GO introduced into the cathode material improved the

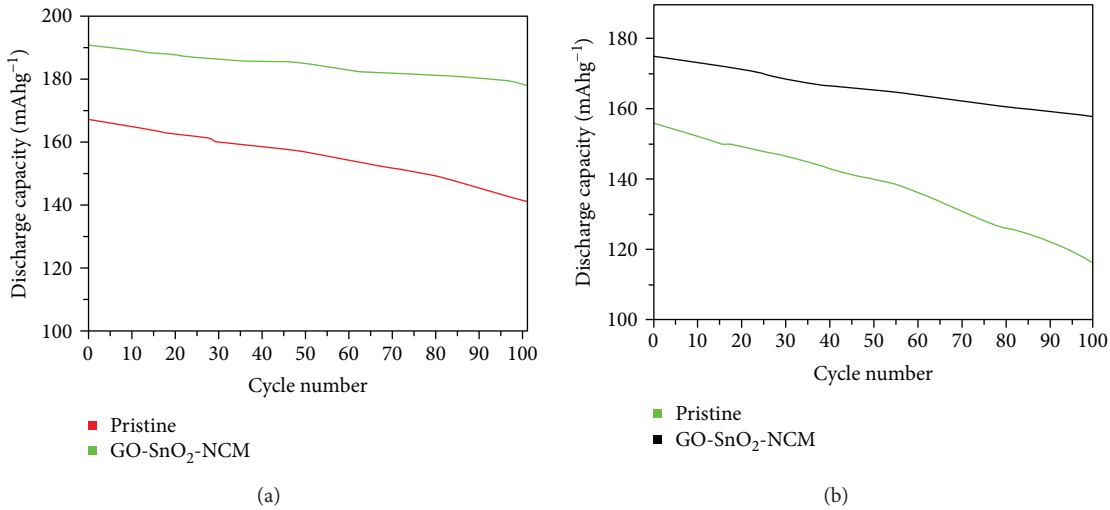

Figure 7: Cycle performance of pristine NCM and GO-SnO_2-NCM samples at 0.2 C (a) for 100 cycles and 1 C (b) for 100 cycles.

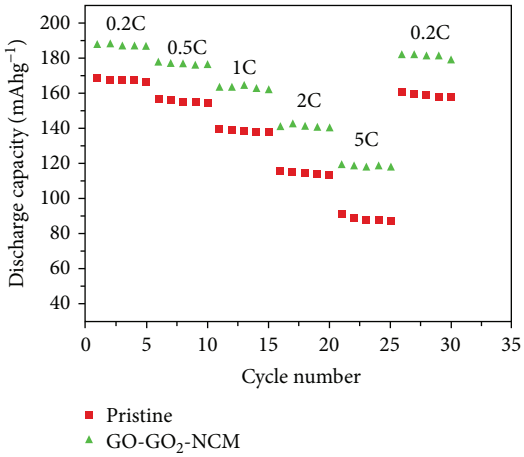

Figure 8: Rate performance of the pristine NCM and GO-SnO_2-NCM samples.

reaction kinetics by increasing the electrical conductivity owing to the GO two-dimensional network. These results suggested strongly that the double-coating layer is a promising method to enhance the rate performance of NCM.

To further study the kinetic differences between pristine NCM and GO-SnO_2-NCM, EIS measurements were performed after 100 discharge cycles. Results showed that the EIS curves comprised a single semicircle in the high-to medium-frequency region and revealed an inclined line in the low-frequency region (Figure 9). Generally, an intercept at the Z′ axis in the high-frequency region corresponded to the solution resistance (R_e). The single semicircle represented the high-to-medium-frequency semicircle, with the frequency representing the charge-transfer resistance (R_{ct}) at the electrode-electrolyte interface [35]. The low-frequency oblique line is related to the lithium-ion diffusion process in the electrode materials, as introduced by Warburg impedance (Z_w) [36]. The equivalent circuit model is shown in Figure 9(b). The values of R_e and R_{ct} were obtained by fitting with ZView software.

In particular, the R_{ct} value of the GO-SnO_2-coated sample increased to 176 Ω, which was smaller than 362 Ω for the pristine material, after 100 cycles, revealing that the double-coated material exhibited better electrochemical performance than the bare NCM did. This indicated that the GO-SnO_2 double-coating layer effectively increased the electrical conductivity and suppressed increases of charge transfer resistance.

The low-frequency oblique line is related to the lithium-ion diffusion process in the electrode materials. The lithium-ion diffusion coefficients (D_{Li}) can be evaluated using the following equations [37, 38]; the explanation of symbols is shown in Table 2:

$$D_{Li} = \frac{R^2T^2}{2A^2n^4F^4C^2\sigma^2}, \quad (1)$$

$$Z' = R_e + R_{sol} + R_{ct} + \sigma\omega^{-(1/2)}. \quad (2)$$

The linear relationship between Z′ and $\omega^{-1/2}$ (square root of the frequency) is in the low-frequency region (Figure 10). Compared to the pristine sample with the lithium-ion diffusion coefficient of 5.29×10^{-13} cm^2/s, the GO-SnO_2-NCM material exhibited a greatly enhanced lithium-ion diffusion coefficient (1.17×10^{-12} cm^2/s). This can be ascribed to the following two factors: first, the SnO_2-coating layer broadened Li^+ insertion/deinsertion during the charge–discharge process and GO with a large surface area increased the content of the unbound cathode material; second, GO-SnO_2 also enhanced the electrical conductivity and facilitated electrolyte movement through the cathode. Therefore, GO-SnO_2-NCM substantially increased the Li^+ diffusion coefficient when compared to pristine materials.

4. Conclusions

GO-coated SnO_2-NCM cathode materials were successfully synthesized via a wet chemical method, and pristine NCM was prepared via a citric acid-assisted sol–gel method. The

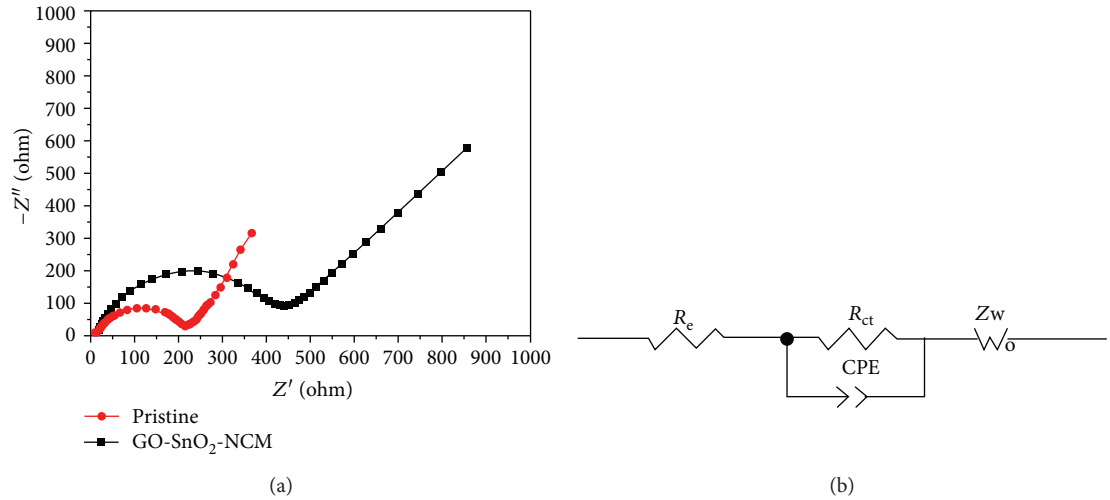

Figure 9: Nyquist plots of NCM and GO-SnO_2-NCM electrodes at 100cycles. (b) Equivalent circuit model, Rct = 362 Ω of NCM; Rct = 176 Ω of GO-SnO_2-NCM.

Table 2: The explanation of symbols.

Symbol	Explanation	Symbol	Explanation
R	The gas constant 8.134 $Jmol^{-1}$ K^{-1}	R_{ct}	The charger transfer resistance
T	The absolute temperature 298.15 K	σ	Warburg factor
A	The surface area of the electrode	R_e	The solution resistance
n	The number of elections per Molecule during oxidization	C	The concentration of lithium ions in the material
F	The Faraday constant 96486 C mol^{-1}	ω	The angular frequency

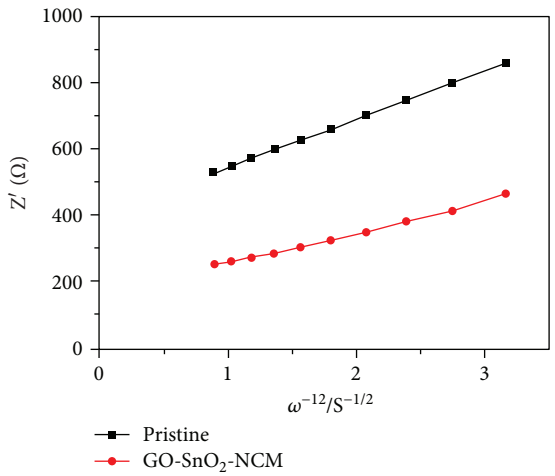

Figure 10: The relationship between Z' and $\omega^{-1/2}(s^{-1/2})$ for NCM and GO-SnO_2-NCM.

double-coating layer was placed on the NCM surface instead of entering into the crystal lattice. In comparison with pristine NCM, GO-SnO_2-NCM showed a much higher discharge capacity, higher rate capability, and higher cycling performance. These improvements are mainly attributed to the GO-SnO_2-coating layer, which can not only protect from HF attacks and electrolyte decomposition but also promote Li^+ conductivity. Therefore, the double-coating layer represents an effective method to overcome the shortcoming of NCM material and a promising candidate for applications in EVs and HEVs.

Data Availability

The data used to support the findings of this study are included within the article.

Conflicts of Interest

The authors declare that they have no conflicts of interest.

Acknowledgments

This work was financially supported by the National Nature Science Foundation of China (Grant No. 51378183), the Research Program of Hubei Provincial Department of Education (T201215), and the Petroleum and Chemical Industry Federation Program of China (Grant Nos. 20171204, 20170902).

References

[1] K. T. Nam, D. W. Kim, P. J. Yoo et al., "Virus-enabled synthesis and assembly of nanowires for lithium ion battery electrodes," *Science*, vol. 312, no. 5775, pp. 885–888, 2006.

[2] C. W. Park, J. H. Ahn, H. S. Ryu, K. W. Kim, and H. J. Ahn, "Room-temperature solid-state sodium/sulfur battery," *Electrochemical and Solid-State Letters*, vol. 9, no. 3, pp. A123–A125, 2006.

[3] V. Paladini, T. Donateo, A. de Risi, and D. Laforgia, "Supercapacitors fuel-cell hybrid electric vehicle optimization and control strategy development," *Energy Conversion and Management*, vol. 48, no. 11, pp. 3001–3008, 2007.

[4] J.-H. Yum, P. Chen, M. Grätzel, and M. . K. Nazeeruddin, "Recent developments in solid-state dye-sensitized solar cells," *ChemSusChem*, vol. 1, no. 8-9, pp. 699–707, 2008.

[5] W. C. Oh and J. Y. Park, "Hydrogen gas generation of metal-activated carbon for fuel cells," *Journal of Industrial and Engineering Chemistry*, vol. 13, pp. 578–584, 2007.

[6] J. M. Tarascon and M. Armand, "Issues and challenges facing rechargeable lithium batteries," *Nature*, vol. 414, no. 6861, pp. 359–367, 2001.

[7] A. Patil, V. Patil, D. Wook Shin, J.-W. Choi, D.-S. Paik, and S.-J. Yoon, "Issue and challenges facing rechargeable thin film lithium batteries," *Materials Research Bulletin*, vol. 43, no. 8-9, pp. 1913–1942, 2008.

[8] T. Eren, N. Atar, M. L. Yola, H. Karimi-Maleh, A. T. Çolak, and A. Olgun, "Facile and green fabrication of silver nanoparticles on a polyoxometalate for Li-ion battery," *Ionics*, vol. 21, no. 8, pp. 2193–2199, 2015.

[9] Y. Takahashi, S. Tode, A. Kinoshita, H. Fujimoto, I. Nakane, and S. Fujitani, "Development of lithium-ion batteries with a $LiCoO_2$ cathode toward high capacity by elevating charging potential," *Journal of the Electrochemical Society*, vol. 155, no. 7, pp. A537–A541, 2008.

[10] A. W. Moses, H. G. G. Flores, J. G. Kim, and M. A. Langell, "Surface properties of $LiCoO_2$, $LiNiO_2$ and $LiNi_{1-x}Co_xO_2$," *Applied Surface Science*, vol. 253, no. 10, pp. 4782–4791, 2007.

[11] A. Eftekhari, "On the fractal study of $LiMn_2O_4$ electrode surface," *Electrochimica Acta*, vol. 48, no. 19, pp. 2831–2839, 2003.

[12] G. Singh, A. Sil, S. Ghosh, and A. Panwar, "Effect of citric acid content on synthesis of $LiNi_{1/3}Mn_{1/3}Co_{1/3}O_2$ and its electrochemical characteristics," *Ceramics International*, vol. 36, no. 6, pp. 1831–1836, 2010.

[13] S. Uchida, N. Zettsu, K. Hirata, K. Kami, and K. Teshima, "High-voltage capabilities of ultra-thin Nb_2O_5 nanosheet coated $LiNi_{1/3}Co_{1/3}Mn_{1/3}O_2$ cathodes," *RSC Advances*, vol. 6, no. 72, pp. 67514–67519, 2016.

[14] K. Araki, N. Taguchi, H. Sakaebe, K. Tatsumi, and Z. Ogumi, "Electrochemical properties of $LiNi_{1/3}Co_{1/3}Mn_{1/3}O_2$ cathode material modified by coating with Al_2O_3 nanoparticles," *Journal of Power Sources*, vol. 269, pp. 236–243, 2014.

[15] S. K. Hu, G. H. Cheng, M. Y. Cheng, B. J. Hwang, and R. Santhanam, "Cycle life improvement of ZrO_2-coated spherical $LiNi_{1/3}Co_{1/3}Mn_{1/3}O_2$ cathode material for lithium ion batteries," *Journal of Power Sources*, vol. 188, no. 2, pp. 564–569, 2009.

[16] J. Li, M. Fan, X. He, R. Zhao, C. Jiange, and C. Wan, "TiO_2 coating of $LiNi_{1/3}Co_{1/3}Mn_{1/3}O_2$ cathode materials for Li-ion batteries," *Ionics*, vol. 12, no. 3, pp. 215–218, 2006.

[17] S. W. Lee, M. S. Kim, J. H. Jeong et al., "Li_3PO_4 surface coating on Ni-rich $LiNi_{0.6}Co_{0.2}Mn_{0.2}O_2$ by a citric acid assisted sol-gel method: improved thermal stability and high-voltage performance," *Journal of Power Sources*, vol. 360, pp. 206–214, 2017.

[18] L. Li, Y. Cao, H. Zheng, and C. Feng, "$AlPO_4$ coated $LiNi_{1/3}Co_{1/3}Mn_{1/3}O_2$ for high performance cathode material in lithium batteries," *Journal of Materials Science: Materials in Electronics*, vol. 28, no. 2, pp. 1925–1930, 2017.

[19] Z. M. Luo, Y. G. Sun, and H. Y. Liu, "Electrochemical performance of a nano SnO_2-modified $LiNi_{1/3}CO_{1/3}Mn_{1/3}O_2$ cathode material," *Chinese Chemical Letters*, vol. 26, no. 11, pp. 1403–1408, 2015.

[20] C. Xu, L. Li, F. Qiu et al., "Graphene oxide assisted facile hydrothermal synthesis of $LiMn_{0.6}Fe_{0.4}PO_4$ nanoparticles as cathode material for lithium ion battery," *Journal of Energy Chemistry*, vol. 23, no. 3, pp. 397–402, 2014.

[21] F. Yu, L. Zhang, L. Lai et al., "High electrochemical performance of $LiFePO_4$ cathode material via in-situ microwave exfoliated graphene oxide," *Electrochimica Acta*, vol. 151, pp. 240–248, 2015.

[22] W. S. Hummers Jr. and R. E. Offeman, "Preparation of graphitic oxide," *Journal of the American Chemical Society*, vol. 80, no. 6, p. 1339, 1958.

[23] N. I. Kovtyukhova, P. J. Ollivier, B. R. Martin et al., "Layer-by-layer assembly of ultrathin composite films from micron-sized graphite oxide sheets and polycations," *Chemistry of Materials*, vol. 11, no. 3, pp. 771–778, 1999.

[24] Y. Ji, Q. Liu, M. Cheng et al., "Facile synthesis of reduced graphene oxide nanosheets by a sodium diphenylamine sulfonate reduction process and its electrochemical property," *Materials Science and Engineering: C*, vol. 33, no. 7, pp. 3811–3816, 2013.

[25] T. Ohzuku, A. Ueda, and M. Nagayama, "Electrochemistry and structural chemistry of $LiNiO_2$ (R_{3m}) for 4 volt secondary lithium cells," *Journal of the Electrochemical Society*, vol. 140, no. 7, pp. 1862–1870, 1993.

[26] S. S. Jan, S. Nurgul, X. Shi, H. Xia, and H. Pang, "Improvement of electrochemical performance of $LiNi_{0.8}Co_{0.1}Mn_{0.1}O_2$ cathode material by graphene nanosheets modification," *Electrochimica Acta*, vol. 149, pp. 86–93, 2014.

[27] K. M. Shaju, G. V. Subba Rao, and B. V. R. Chowdari, "Performance of layered $Li(Ni_{1/3}Co_{1/3}Mn_{1/3})O_2$ as cathode for Li-ion batteries," *Electrochimica Acta*, vol. 48, no. 2, pp. 145–151, 2002.

[28] A. M. A. Hashem, A. E. Abdel-Ghany, A. E. Eid et al., "Study of the surface modification of $LiNi_{1/3}Co_{1/3}Mn_{1/3}O_2$ cathode material for lithium ion battery," *Journal of Power Sources*, vol. 196, no. 20, pp. 8632–8637, 2011.

[29] P. Manikandan and P. Periasamy, "Novel mixed hydroxy-carbonate precursor assisted synthetic technique for $LiNi_{1/3}Mn_{1/3}Co_{1/3}O_2$ cathode materials," *Materials Research Bulletin*, vol. 50, pp. 132–140, 2014.

[30] K. Amine, H. Tukamoto, H. Yasuda, and Y. Fujita, "A new three-volt spinel $Li_{1+x}Mn_{1.5}O_4$ for secondary lithium batteries," *Journal of the Electrochemical Society*, vol. 143, no. 5, pp. 1607–1613, 1996.

[31] D. Wang, X. Li, Z. Wang et al., "Improved high voltage electrochemical performance of Li_2ZrO_3-coated $LiNi_{0.5}Co_{0.2}Mn_{0.3}O_2$ cathode material," *Journal of Alloys and Compounds*, vol. 647, pp. 612–619, 2015.

[32] X. Chen, D. Chu, L. Wang et al., "One-step synthesis of novel hierarchical flower-like SnO_2 nanostructures with enhanced photocatalytic activity," *Journal of Alloys and Compounds*, vol. 729, pp. 710–715, 2017.

[33] Q. Liang, L. Zhang, M. Cai et al., "Preparation and characterization of Pt/functionalized graphene and its electrocatalysis

for methanol oxidation," *Electrochimica Acta*, vol. 111, pp. 275–283, 2013.

[34] S. Yang, X. Wang, X. Yang et al., "Determination of the chemical diffusion coefficient of lithium ions in spherical $Li[Ni_{0.5}Mn_{0.3}Co_{0.2}]O_2$," *Electrochimica Acta*, vol. 66, pp. 88–93, 2012.

[35] Q. Wang, N. Tian, K. Xu et al., "A facile method of improving the high rate cycling performance of $LiNi_{1/3}Co_{1/3}Mn_{1/3}O_2$ cathode material," *Journal of Alloys and Compounds*, vol. 686, pp. 267–272, 2016.

[36] S. J. Shi, J. P. Tu, Y. Y. Tang, Y. Q. Zhang, X. L. Wang, and C. D. Gu, "Preparation and characterization of macroporous $Li_{1.2}Mn_{0.54}Ni_{0.13}Co_{0.13}O_2$ cathode material for lithium-ion batteries via aerogel template," *Journal of Power Sources*, vol. 240, pp. 140–148, 2013.

[37] N. Takami, A. Satoh, M. Hara, and T. Ohsaki, "Structural and kinetic characterization of lithium intercalation into carbon anodes for secondary lithium batteries," *Journal of the Electrochemical Society*, vol. 142, no. 2, pp. 371–379, 1995.

[38] A. J. Bard and L. R. Faulkner, *Electrochemical Methods*, Wiley, 2nd edition, 2001.